Mean-scatterer spacing estimates with spectral correlation

Tomy Varghese and Kevin D. Donohue
Department of Electrical Engineering, University of Kentucky, Lexington, Kentucky 40503

An ultrasonic backscattered signal from material comprised of quasiperiodic scatterers exhibit redundancy over both its phase and magnitude spectra. This paper addresses the problem of estimating mean-scatterer spacing from the backscattered ultrasound signal using spectral redundancy characterized by the spectral autocorrelation (SAC) function. Mean-scatterer spacing estimates are compared for techniques that use the cepstrum and the SAC function. A-scan models consist of a collection of regular scatterers with Gamma distributed spacings embedded in diffuse scatterers with uniform distributed spacings. The model accounts for attenuation by convolving the frequency dependent scattering centers with a time-varying system response. Simulation results indicate that SAC-based estimates converge more reliably over smaller amounts of data than cepstrum-based estimates. A major reason for the performance advantage is the use of phase information by the SAC function, while the cepstrum uses a phaseless power spectral density that is directly affected by the system response and the presence of diffuse scattering (speckle). An example of estimating the mean-scatterer spacing in liver tissue also is presented.

PACS numbers: 43.60.Cg, 43.80.Cs

INTRODUCTION

Ultrasonic backscattered signals from biological tissue contain information regarding resolvable scatterer structures. The information, however, is corrupted by echoes from diffuse (unresolvable) scatterers.[1] This paper examines characterizing tissue microstructure variations with the spectral correlation components of the backscattered signal. The spectral autocorrelation (SAC) function provides an estimate of the mean-scatterer spacing that uses phase information to reduce the degradation caused by the system effects and the presence of diffuse scatterers.[2-7] It has been shown that increasing regularity of the scatterer spacing gives rise to well-defined local maxima among the correlation components in the SAC function.[4,5] This paper demonstrates superior performance for spectral correlation methods over methods that simply use the power spectral density (PSD).

The mean-scatterer spacing parameter has been proposed for tissue characterization. Fellingham and Sommer[8] used mean-scatterer spacing to differentiate between normal and cirrhotic liver. Their algorithm was based on the detection of spectral peaks in the PSD. The cepstrum was initially used for tissue characterization by Kuc[9] in order to reduce the system effects in the PSD. Performance comparisons between cepstral methods for detecting the mean scatterer spacing[10] showed that the AR model performs better than FFT methods for smaller gate lengths. Wagner et al.[11,12] proposed the use of three scatterer features to classify tissue architecture: the mean-scatterer spacing, the ratio of specular to diffuse scatterer intensities, and the fractional standard deviation in the specular scatterers. Intensity (squared envelope) images were used to estimate the individual contributions of diffuse and regular scattering to the overall intensity. The scatterer spacing was estimated from the power spectrum of the intensity by a weighted thresholding procedure.

This work models soft tissue as an acoustic medium containing two types of scatterers. The first component is the diffuse scatterers, which are uniformly distributed throughout the tissue and are of a sufficient number to generate an echo signal with circular Gaussian statistics.[11,12] The second class of scatterers have regularity associated with them and contribute to the specular echoes in the backscattered ultrasound signal. This paper models the spacings between these regular scatterers with a Gamma distribution. The Gamma distribution provides a flexible method for simulating parametric regularity in the scatterer spacing. Landini and Verrazini[13] demonstrated that both average interval spacing and the variance of the spacing could be parametrically described using a Gamma distribution. The mean and variance of the scatterer spacings were estimated from the periodicity and attenuation of the cepstral peaks. The aim of this paper is to demonstrate the advantages of using spectral redundancy in estimating the mean-scatterer spacing. This paper compares the estimation performance enhancement attained using a spectral redundancy technique (SAC), relative to a cepstral analysis technique using the PSD.[10]

A brief description of the mean-scatterer spacing estimators are discussed in Sec. I. Section II discusses the simulation experiment and analyzes the relative merits of the techniques used in determining the scatterer spacing. Application of these methods to in vivo data from liver tissue is discussed in Sec. IV. Finally, Sec. V summarizes the significance of the results obtained to tissue characterization using ultrasound.

I. THEORY

The tissue model consists of a sparse collection of randomly distributed, weak scattering particles that interact with

the incident pulse only once (multiple scattering is assumed to be negligible). The tissue scatterers within the ultrasonic beam field can be written as

$$x(t) = \sum_{n=1}^{N_S} a_n(t - \tau_n) + \sum_{n=1}^{N_D} \nu_n(t - \theta_n). \tag{1}$$

where t is a time axis (related to the distance by the velocity of the pulse), N_D is the total number of diffuse scatterers, ν_n denotes the reflectivity of the nth diffuse scatterer, θ_n represents the delay associated with the nth diffuse scattering center, N_S is the total number of regular scatterers, a_n denotes the reflectivity of the nth regular scatterer, and τ_n represents the delay associated with the nth regular scattering center.

The attenuation of the propagating ultrasound pulse depends on the scattering and absorption properties of the tissue. The impulse response due to the system and propagation path (to and from the scatterer field), is represented by a time varying system response function $h(t, \tau)$. The impulse response changes with time due to the frequency dependent attenuation of the pulse as it propagates through the tissue. The A-scan corresponding to the scattered field can now be written as

$$y(t) = \int_{-\infty}^{\infty} h(t, \tau) \left(\sum_{n=1}^{N_S} a_n(\tau - \tau_n) \right. $$
$$\left. + \sum_{n=1}^{N_D} \nu_n(\tau - \theta_n) \right) d\tau, \tag{2}$$

where τ, the variable of integration, represents the system response axis at a given time t.

For nonstationary signal analysis, the periodogram and the SAC functions are computed over small windowed segments of the A-scan with a data tapering Welch window, using the Welch–Bartlett technique.[18] Detectability of the mean-scatterer spacing requires the presence of at least two regular scatterers within the window (i.e., $T > \Delta$, where Δ is the mean-regular scatterer spacing and T is the window length). Adjacent overlapping data segments are averaged (Welch–Bartlett technique[18]) to obtain the PSD and SAC function estimates from the A scan. A single windowed segment is denoted by

$$y_T \left(\tau; t - u \frac{T}{J} \right)$$
$$= \begin{cases} y \left(\tau - t + u \frac{T}{J} \right) w_T(\tau), & -\dfrac{T}{2} \leq \tau \leq \dfrac{T}{2}, \\ 0, & \text{elsewhere} \end{cases} \tag{3}$$

where $y_T(\cdot)$ represents a tapered data segment centered at $t - uT/J$ of finite duration T, $w_T(\cdot)$ represents the tapered

window, and J represents the amount of overlap between the uth and $u+1$th tapered data segment (i.e., $(1 - 1/J) \times 100$ is the percent overlap between segments for $1 \leq J < \infty$). Let N'_S and N'_D denote the number of regular and diffuse scatterers that contribute to the A-scan segment over the interval T. The Fourier transform of Eq. (3) with respect to τ, at a given time t, can be written as

$$Y_T \left(f; t - u \frac{T}{J} \right) = H(f; t) \left(\sum_{n=1}^{N'_S} A_n(f) e^{-j2\pi f \tau_n} \right.$$
$$\left. + \sum_{n=1}^{N'_D} V_n(f) e^{-j2\pi f \theta_n} \right), \tag{4}$$

where f is frequency, $H(f)$ and $Y(f)$ are the Fourier transforms of $h(\tau)$ and $y(\tau)$, respectively, and $A_n(f)$ and $V_n(f)$ denote the frequency dependent scattering strength of scatterer $a_n(\tau)$ and $\nu_n(\tau)$, respectively.

A. The spectral autocorrelation function

The phase and magnitude spectrum of backscattered energy from regularly spaced scatterers contains information related to the spacing mean and variance. While the PSD can be used to characterize the scatterer spacing, it relies only on the magnitude spectrum, which is directly affected by the system response and diffuse scattered energy. The SAC function, however, uses information in the phase spectrum, which results in local maxima in the bifrequency plane where the mean contributions of the diffuse scatterer energy is zero (this is not the case for the PSD). As a result, the SAC function provides a more robust estimate than the PSD for scatterer spacing in the presence of diffuse scattering. These points are illustrated in this section by defining the SAC function and deriving a relationship between the regular and diffuse scatterer distributions and local maxima in the SAC function.

The SAC function[2] is defined over a bifrequency plane by

$$S_T(f_1, f_2; t) = E[Y_T(f_1; t) Y_T^*(f_2; t)]$$
$$\approx \frac{1}{L + 1} \sum_{u = -L/2}^{L/2} Y_T \left(f_1; t - u \frac{T}{J} \right)$$
$$\times Y_T^* \left(f_2; t - u \frac{T}{J} \right), \tag{5}$$

where $Y_T(\cdot)$ is the Fourier transform of the windowed A-scan segment, and $Y_T^*(\cdot)$ is its complex conjugate. The approximation to the expected value is denoted by the average of $L + 1$ local segments. The relationship between the SAC function and the scatterer configurations is seen by substituting in $Y_T(\cdot)$ from Eq. (4), and assuming the attenuation of the pulse over the region of interest, defined by t and L is negligible

$$S_T(f_1,f_2;t)=H(f_1;t)H^*(f_2;t)\times E\left[\sum_{n=1}^{N'_S}\sum_{m=1}^{N'_S}A_n(f_1)A_m^*(f_2)e^{-j2\pi(f_1\tau_n-f_2\tau_m)}+\sum_{n=1}^{N'_S}\sum_{m=1}^{N'_D}A_n(f_1)V_m^*(f_2)e^{-j2\pi(f_1\tau_n-f_2\theta_m)}\right.$$

$$\left.+\sum_{n=1}^{N'_D}\sum_{m=1}^{N'_S}V_n(f_1)A_m^*(f_2)e^{-j2\pi(f_1\theta_n-f_2\tau_m)}+\sum_{n=1}^{N'_D}\sum_{m=1}^{N'_D}V_n(f_1)V_m^*(f_2)e^{-j2\pi(f_1\theta_n-f_2\theta_m)}\right]. \tag{6}$$

Under the assumption that the diffuse scatterer sizes and positions are uncorrelated with the regular scatterers, the expected value of the summation cross-product terms between the diffuse and regular scatterers in Eq. (6) reduces to zero

$$S_T(f_1,f_2;t)$$

$$=H(f_1;t)H^*(f_2;t)$$

$$\times\left(E\left[\sum_{n=1}^{N'_S}\sum_{m=1}^{N'_S}A_n(f_1)A_m^*(f_2)e^{-j2\pi(f_1\tau_n-f_2\tau_m)}\right]\right.$$

$$\left.+E\left[\sum_{n=1}^{N'_D}\sum_{m=1}^{N'_D}V_n(f_1)V_m^*(f_2)e^{-j2\pi(f_1\theta_n-f_2\theta_m)}\right]\right). \tag{7}$$

Since the diffuse scatterer sizes and positions are uncorrelated with each other, cross-scatterer terms in the second summation term become zero {i.e., $E[V_n(f_1)V_m^*(f_2)\times e^{-j2\pi(f_1\theta_n-f_2\theta_m)}]=0$, $m\neq n$]. In addition, if the diffuse scatterer process is wide-sense stationary over the region of interest, the terms where $f_1\neq f_2$ are also uncorrelated.[19] Thus, Eq. (7) can be rewritten as

$$S_T(f_1,f_2;t)$$

$$=H(f_1;t)H^*(f_2;t)$$

$$\times\left(E\left[\sum_{n=1}^{N'_S}\sum_{m=1}^{N'_S}A_n(f_1)A_m^*(f_2)e^{-j2\pi(f_1\tau_n-f_2\tau_m)}\right]\right.$$

$$\left.+\sum_{n=1}^{N'_D}E[V_n(f_1)V_n^*(f_2)]\delta(f_1-f_2)\right). \tag{8}$$

Since the frequency components of the diffuse scatterer echo signal are uncorrelated, they contribute only to the diagonal of the SAC function, which is the PSD of the diffuse component. Thus, the expected value of the diffuse scatterer components do not contribute to the off-diagonal components of the SAC function.

To create a variable related to the scatterer spacing, the following substitution is made

$$\Delta_i=\frac{\tau_i}{i}. \tag{9}$$

The ith scatterer position is represented by i equal intervals from the beginning of the segment. This change of variables gives a good approximation to the actual spacing when the scatterer spacing variance is small. For the extreme case where the scatterer spacing is constant, $\Delta_i=\Delta$, Eq. (8) can be expressed as:

$$S_T(f_1,f_2;t)$$

$$=H(f_1;t)H^*(f_1;t)$$

$$\times\left(E\left[\sum_{n=1}^{N'_S}\sum_{m=1}^{N'_S}A_n(f_1)A_m^*(f_2)e^{-j2\pi\Delta(f_1n-f_2m)}\right]\right.$$

$$\left.+\sum_{n=1}^{N'_D}E[V_n(f_1)V_n^*(f_2)]\delta(f_1-f_2)\right). \tag{10}$$

The regular scatterer summation in Eq. (10) indicates when f_1n-f_2m equals integer multiples of $1/\Delta$ for all m and n, the individual terms in the summation are in phase and local maxima occur at these points. The maxima occur both along the PSD axis, where $f_1=f_2=k/\Delta$, and throughout the rest of the SAC function, where $f_1-f_2=k/\Delta$ (for $k=\pm1,2,3,...$). When the regular scatterer spacings are randomly (Gamma) distributed, similar local maxima occur. These maxima, however, are less pronounced for greater variance in the scatterer spacings.[6]

In the cepstral approach for estimating mean-scatterer spacing, the system effect is reduced from the scatterer component by taking the logarithm of Eq. (10) (to change multiplicative relationships to additive), and then applying high-pass filtering.[13] The diffuse component, however, is not separated from the regular component in this process, since they remain together in the argument of the logarithm term. On the other hand, the spectral region of the SAC function where $f_1\neq f_2$ contains no contribution from the diffuse scatterers. Therefore, when the SAC function is computed from the data, the off-diagonal terms result in higher regular-to-diffuse scatterer signal ratio than the diagonal terms (PSD components) after sufficient averaging.

A normalization for the SAC function provides a way of minimizing the amplitude variations due the system and propagation effects. The normalization is given by

$$P(f_1,f_2)=S(f_1,f_2)/\sqrt{S(f_1,f_1)S(f_2,f_2)}, \tag{11}$$

where $P(f_1, f_2)$ denotes the correlation coefficient. Note the resulting diagonal of the normalized SAC function is unity. Thus, all the information regarding scatterer spacing is in the off-diagonal components of the normalized SAC function, and amplitude variations in the spectrum due to systems effects are eliminated.

Normalization was not used previously by Varghese and Donohue,[4] where the smallest scatterer spacing was determined graphically by the spectral correlation peak farthest away from the PSD diagonal. In the case of very regular tissue other spectral peaks occur closer to the PSD diagonal that correspond to larger scatterer spacings harmonically related to the smaller spacing. Due to the amplitude variation in the spectrum from the system response, spectral correlation peaks closer to the PSD diagonal have larger magnitudes as a result of their corresponding spectral components being closer to the center of the system bandwidth. Since the normalization used in Eq. (11) divides the spectral correlation peak magnitude by the square root of the product of the magnitudes of its corresponding components along the PSD, the magnitude variations from the system are effectively removed, and correlation peaks which remain are due to the coherence in the phase information.

It should be noted that the magnitude variations in the PSD diagonal due to the scatter spacings are also eliminated by this normalization. The phase information, however, is sufficient to generate local maxima in the bifrequency plane for detecting the scatterer spacing. Thus, normalization of the SAC function allows for consistent detections of the spectral correlation peak location irrespective of the distance from the PSD. A simple numerical algorithm can be used to detect the maximum peak in the off-diagonal components (i.e., visual inspection of the SAC function is not necessary).

Since normalization is performed in the frequency domain and the system is band limited, useful information about the scatterer spacing is determined by the pulse width. To avoid amplifying low signal-to-noise (SNR) spectral regions, normalization is performed only in the region where significant energy is present in the PSD (typically the 3–6 dB region of the received signal spectrum). Spurious peaks will occur if low SNR regions are included in the normalization window (i.e., usually below the 10-dB bandwidth of the received pulse). These peaks will result in scatterer spacings being detected near or beyond the resolution limit of the system when no regular scatterer spacing is present in the tissue.

B. The power spectrum

Classical methods of estimating the power spectrum are based on the periodogram. The PSD is defined by

$$P_T(f) = E[|Y_T(f;t)|^2]$$

$$\approx \frac{1}{L+1} \sum_{u=-L/2}^{L/2} \left| Y_T\left(f; t - u\frac{T}{J}\right) \right|^2,$$ (12)

where $L + 1$ is the number of segments averaged. The rela-

tionship between the PSD and the scatterers is obtained from Eq. (8) by substituting $f_1 = f_2 = f$, to obtain

$$P_T(f) = H(f;t)H^*(f;t)$$

$$\times \left(E\left[\sum_{n=1}^{N_S'} \sum_{m=1}^{N_S'} A_n(f)A_m^*(f)e^{-j2\pi f(\tau_n - \tau_m)} \right] \right.$$

$$\left. + \sum_{n=1}^{N_D'} E[V_n(f)V_n^*(f)] \right).$$ (13)

Using the change of variables in Eq. (9), with a constant scatterer spacing $\Delta_i = \Delta$, Eq. (13) reduces to

$$P_T(f) = H(f;t)H^*(f;t)$$

$$\times \left(E\left[\sum_{n=1}^{N_S'} \sum_{m=1}^{N_S'} A_n(f)A_m^*(f)e^{-j2\pi \Delta f(n - m)} \right] \right.$$

$$\left. + \sum_{n=1}^{N_D'} E[V_n(f)V_n^*(f)] \right).$$ (14)

We can see from Eq. (14), for the regular scatterers, that if f is a multiple of $1/\Delta$, all the summation terms are in phase and local maxima occur in the PSD. These periodic peaks in the PSD have been used directly for determining the average scatterer spacing in very regular tissue.[8–10,13]

C. The cepstrum

Periodicity in the PSD produces a dominant peak in the cepstrum, which is used to determine the scatterer spacing. The cepstrum is the most commonly used method to detect the scatterer spacing. The cepstrum is defined as the Fourier transform of the logarithm of the PSD. The logarithm of Eq. (14) results in

$$\log P_T(f) = \log[H(f;t)H^*(f;t)]$$

$$+ \log\left(E\left[\sum_{n=1}^{N_S'} \sum_{m=1}^{N_S'} A_n(f)A_m^*(f)e^{j2\pi \Delta f(n - m)} \right] \right.$$

$$\left. + \sum_{n=1}^{N_D'} E[V_n(f)V_n^*(f)] \right).$$ (15)

Cepstral processing assumes slow variations for the system response [first log term in Eq. (15)] with respect to the variations in the regular scatterer spacing [second log term in Eq. (15)]. As a result, the log of the system response is reduced (using a high-pass filter) and the inverse Fourier transform is taken. The scatterer spacing periodicity now manifests itself as peaks at integer multiples of Δ, with the dominant peak at Δ. The dominant peak is used to determine the mean-scatterer spacing in tissue.[10] Observe also from Eq. (15) that the PSD resulting from the diffuse scatterers adds directly to the regular scatterer component within the argument of the logarithm. As a result, simple spectral filtering

will not directly reduce this degradation of the cepstrum for regular scatterers.

The mean-scatterer spacing is computed from the location (Δt) of the dominant peak in the cepstrum estimated from the PSD. For the SAC function, the location of the dominant peak among the off-diagonal spectral components at (f_1, f_2), corresponds to a frequency difference $(\Delta f = f_1 - f_2)$ that is used to compute the mean scatterer spacing

$$d = \frac{V}{2\Delta f} = \frac{1}{2} V\Delta t, \tag{16}$$

where V denotes the velocity of propagation of the ultrasound pulse.

The finite bandwidth, of the interrogating pulse imposes limitations on the average scatterer spacing which can be resolved by the imaging system. The mean-scatterer spacing is resolved, if the correlation length of the system impulse response is shorter than the spacing between the individual scatterers. For scatterers not resolved by the system, local maxima corresponding to scatterer spacing is not observed. Simulation results for the case of unresolvable scatterers have shown relationships between the average spectral correlation (average of all correlation term magnitudes in off-diagonal region) and the unresolvable scatterer density.[22] When no regularity is present in scatterers, the dominant peak tends to occur near the first off-diagonal (due to leakage from the PSD).

This section presented different methods used to detect the scatterer spacing. Cepstral techniques require high-pass filtering to reduce the system effect from the tissue signature, which involves setting a cutoff frequency for the filter. The cutoff frequency can be set to pass the minimum detectable scatterer spacing (i.e., on the order of the pulse width) or higher, if the range of scatterer spacing of interest is known. The SAC function does not require high-pass filtering, however, a frequency window must be applied before normalization to ensure information is taken only from the spectral region of the imaging system. The estimation technique using the SAC function detects the location of the dominant off-diagonal component, and uses this information to compute the scatterer spacing. Simulation results presented in the next section show the performance improvement obtained using the SAC function to detect periodicities in the presence of diffuse backscatter and varying regularity in the regular scatterers.

II. SIMULATION

A-scans with known tissue and signal parameters are simulated using Eqs. (2) and (4). The simulator parameters were chosen within the range of values reported in literature from experimental research with different types of tissue *in vitro*.[15–17] The size of the quasiperiodic (regular) scatterers was constant for all the simulations. Scatterer sizes influence the frequency dependence of the pulse scattering and attenuation for the propagating ultrasonic pulse. The scatterer size for the regular component of the scattering was chosen as 80 μm. The Gamma function was used to describe the scatterer

distribution for regular scattering. Scatterer spacings were simulated from cases with a very irregular spacing (large standard deviation), to cases with almost deterministic spacings (corresponding to Gamma orders from 50–1000, respectively). The diffuse component was modeled using a uniform distribution for scatterers (size 10 μm) with the scatterer density chosen to simulate Gaussian statistics for the scatterer number (about 15–20 scatterers per resolution cell using a Poisson distribution). The absorption coefficient was chosen as 0.94-dB cm^{-1} (corresponds to measured values for liver tissue) and a diffuse-differential scattering coefficient of 9×10^{-4} cm^{-1} sr^{-1} for backscattering at an angle of 180°, measured at 3 MHz.[17]

The pulse parameters are used to obtain the initial system response $h(t)$ which is modified as the pulse propagates through the microstructure due to the frequency dependent attenuation. The interrogating pulse was simulated with a center frequency of 3.5 MHz and a Gaussian shaped envelope. The propagation velocity of the pulse through biological tissue was set at 1540 m/s. The bandwidth of the pulse should be at least $1/\Delta$, in order to observe spectral peaks due to the distribution of the scatterers in the microstructure. The simulated pulse had a 3-dB bandwidth of 1.9 MHz, which limited the minimum detectable scatterer spacing to 0.41 mm.

The regular scattering component was simulated with a scatterer spacing of 0.51 mm. A gate length (T) of 4 mm or 128 data points was used to form the PSD and the SAC function estimates. The mean-scatterer spacing was estimated from the FFT cepstrum. The cepstrum was filtered using a high-pass filter with cutoff frequency 1.5 MHz to reduce system effects. The scatterer spacing was also estimated from the location of the largest off-diagonal peak of the SAC function. The simulation was performed for regular scatterers with different spacing variances and different strengths of the diffuse component.

When estimating the SAC function, with a hopping window, a phase correction factor is helpful for correcting the phase difference between regular scatterer positions and the center of the window. For regularly spaced scatterers the relative phase difference between the center of the window and the scatterer location degrade the coherent sums in the off-diagonal regions of the SAC function. When consecutive SAC functions are averaged, the phase difference between the center of the window and the scatterer location impedes the convergence of the SAC function. This error makes a significant difference when only a few regular scatterers exist over the data segment window. When the regular scatterers are more dense within the processing window, the phase difference between a regular scatterer and the center of the window is small, and therefore does not significantly hinder the convergence.

The phase correction factor for each tapered data segment aligns the regular scatterers with the center of the window. The proper phase shift is determined by the distance of any regular scatterer location to the center of the window. With the phase correction factor included, Eq. (14) can be written as
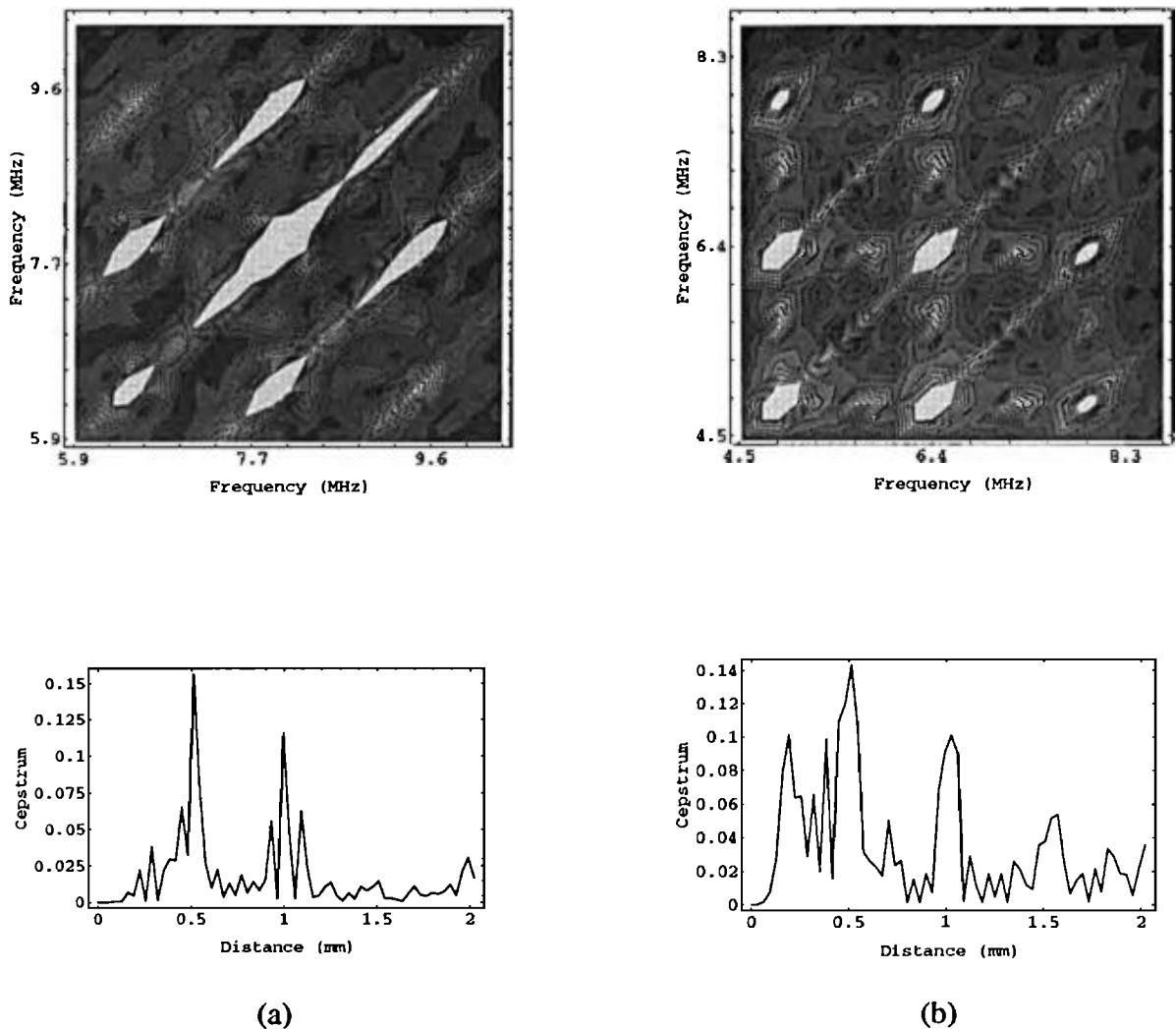
FIG. 1. Spectral autocorrelation function, and FFT cepstrum for scatterers with a 0.51-mm-mean-scatterer spacing with $\sigma=3.15\%$. (a) Only regular scatterers, (b) with a +3-dB-diffuse component relative to the regular scatterers.

$$P_T\!\left(f;t-u\,\frac{T}{J}\right)=Y_T\!\left(f;t-u\,\frac{T}{J}\right)e^{j2\pi f(\tau_{N_s}-T/2)}, \qquad (17)$$

where τ_{N_s} represents the location of any regular scatterer, and $P_T(\cdot)$ is the phase corrected Fourier transform of the windowed A-scan segment (for practical application the maximum value within a data segment is assumed to be the location of a regular scatterer, which is used to obtain τ_{N_s}). The linear phase correction factor does not affect the location of the off-diagonal peaks, it merely aligns the window with the scatterer structure, and helps in the coherent phase addition during the averaging of consecutive overlapped SAC functions. The phase corrected SAC function using Eqs. (17) and (10) can be written as

$$S_T(f_1,f_2;t)\simeq\frac{1}{L+1}\sum_{u=-L/2}^{L/2}P_T\!\left(f_1;t-u\,\frac{T}{J}\right)$$

$$\times P_T^*\!\left(f_2;t-u\,\frac{T}{J}\right)e^{j2\pi(f_1-f_2)(\tau_{N_s}-T/2)}.$$

$$(18)$$

Sample plots of the unnormalized SAC function and the cepstrum are presented in Fig. 1 for regular scatterers with $\sigma=3.15\%$ (standard deviation relative to the mean-scatterer spacing). Figure 1(a) shows a contour plot of the SAC function and the cepstrum for regular scatterers only, while Fig. 1(b) shows the effect of +3 dB of the diffuse component in addition to the regular scatterers. The contour plots are thresholded to emphasize the local maxima. The light intensity regions are those that exceeded the threshold to indicate a local maxima. The 0.51-mm-regular scatterer spacing is easily identified in the cepstrum Fig. 1(a) and (b). Note the presence of a periodicity at 1 mm, which is harmonically related to the 0.5-mm scatterer spacing. The diffuse component directly adds to the PSD, as was discussed in Eq. (15), and causes a broadening of the cepstral peaks, and an increase in the number of spurious peaks as seen in Fig. 1(b). For the SAC function the mean-scatterer spacing is estimated from the location of the off-diagonal peak at (7.75, 6.24) MHz, which corresponds to $\Delta f=1.51$ MHz. Substitute this value into Eq. (16) to obtain a scatterer spacing of 0.51 mm. The spectral correlation peak for the SAC function with the
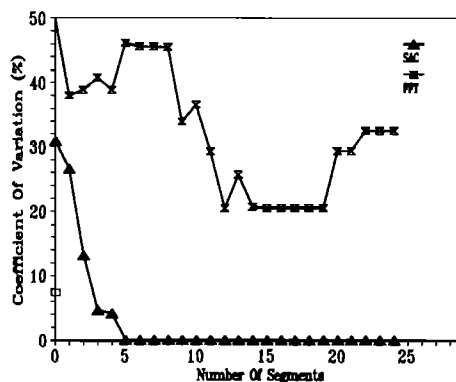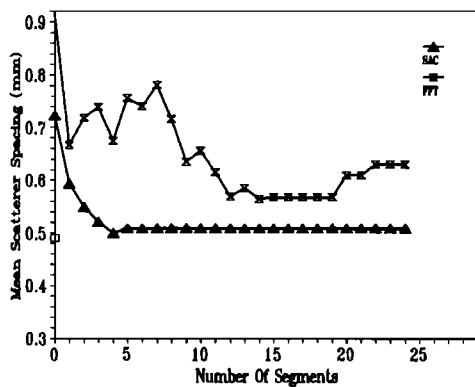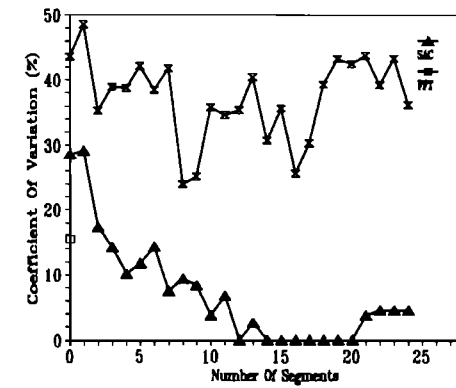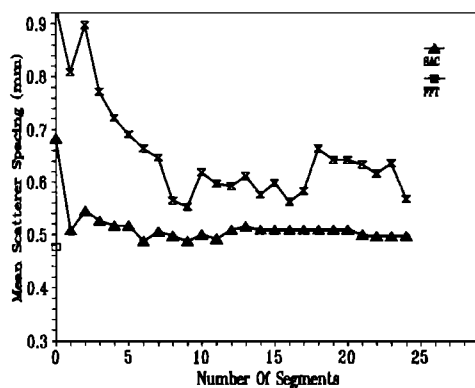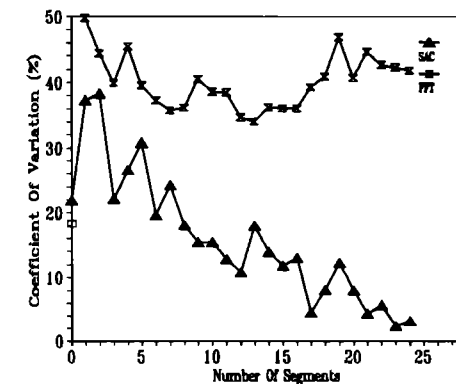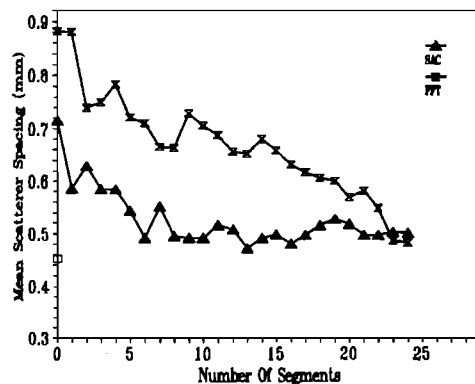
FIG. 2. Mean-scatterer spacing and the coefficient of variation for regular scatterers with spacing 0.51 mm. (a) Standard deviation 0.016 mm (3.15%), (b) standard deviation 0.051 mm (9.99%), (c) standard deviation 0.072 mm (14.14%).

diffuse component is at (4.9, 6.4) MHz, which corresponds to $\Delta f = 1.50$ MHz, giving a scatterer spacing of 0.51 mm.

Monte Carlo simulations were used to compare the performance between the SAC and FFT cepstrum estimates of the mean-scatterer spacing. Convergence plots for the scatterer spacing estimate used 25 independent simulated A-scans with the same tissue and signal parameters. The A-scans were generated with gamma distributed random variables for the regular scatterer spacing. The diffuse scatterers were uniformly distributed throughout the microstructure with uniformly distributed scatterer strengths. The PSD and the SAC functions were computed using a hopping window with 4-mm length, and a 50% ($J=2$) overlap of the tapered data segments along the A-scan. The spectrum at each window location was averaged with the previous spectra to obtain an estimate for the PSD and the SAC function.

Both the computed mean scatterer spacing (d) and the coefficient of variation (CV) of the spacing estimates are presented in Figs. 2 and 3 for increasing standard deviations in the regular scatterer spacing distribution. The coefficient of variation was computed as the ratio of the standard deviation of the estimates to the mean estimate computed over the results from the 25 simulated A-scans.

Figure 2 presents the mean-scatterer spacing and the CV for only quasiperiodic scatterers (no diffuse scattering), as a function of the number of A-scan segments used. The plots show that the estimates obtained using the SAC function converges faster than the cepstral technique and has a lower CV. In Fig. 2(a) the SAC function mean-scatterer spacing estimate (with $\sigma=3.15\%$) converges within 6 averages (corresponding to 14.4 mm or nearly four full data segments), while the cepstral technique converges in about 14 averages with a small bias (i.e., less than 10%). The CV also reduces to 0.0% for the SAC function within 6 averages. A major source of deterioration in the performance of the cepstral technique with no noise, is due to the presence of the harmonic at 1 mm, whose peak dominates for some A scans.

With an increase in the standard deviation of the regular scatterer spacing, the results in Fig. 2(b) and (c) show a slower convergence to the mean-scatterer spacing. In Fig. 2(b) the SAC function CV is within 5% after 14 averages, for $d=0.50$ mm with $\sigma=9.99\%$. In Fig. 2(c) the SAC function CV is within 10% with $d=0.48$ mm for $\sigma=14.14\%$. In both Fig. 2(b) and (c) the CV for the cepstral technique is at about 40%, with the mean-scatterer spacing ranging from 0.55 to 0.65 mm. Results in Fig. 2(b) and (c) indicate the SAC function estimate is more accurate and reliable than the cepstrum.

Estimation of the scatterer spacing in the presence of strong diffuse scattering is presented in Fig. 3 with the ratio of the diffuse to regular scatterer strength at +3 dB (i.e., +3 dB of the diffuse component is added to the regular component of the A scan). Figure 3(a) to (c) show the effect of the change in the microstructure regularity in the presence of diffuse scattering. The SAC function is able to resolve the regular scatterer spacing even in the presence of the diffuse component with no significant degradation in performance of the SAC function [compare Figs. 2(a) and 3(a)]. In the presence of the diffuse component the SAC function estimate fluctuates about the true scatterer spacing by 0.03 mm for $\sigma=9.9\%$, and by 0.06 mm for $\sigma=14.14\%$, with the CV increasing to 6% and 10%, respectively [compare Fig. 2(b) and (c) to Fig. 3(b) and (c)].

Note the cepstral technique converges to a scatterer spacing value close to the cutoff frequency of the high-pass filter for regular scatterers with σ between 9.9% to 14.14%. The cepstral estimates converges to this region because of the contribution of the spurious peaks at lower frequencies and the larger scatterer spacing variance, which reduces the cepstral peak corresponding to the regular scatterer spacing [observe in Fig. 1(b), the presence of strong spurious peaks near values below 0.51 mm]. In addition, the diffuse component adds directly to the PSD corresponding to the regular scatterer structures and causes a broadening of the cepstral peaks along with other effects due to the nonlinear operation (logarithm) on the sum of the two components. The CV in

this case reduces because the spurious peaks near the filter cutoff frequency are consistently detected. This is not an indication of good performance since the estimation is converging on the incorrect value. The diffuse component thus introduces spurious peaks in the cepstrum and reduces the contribution of the regular scatterers to the true cepstral peak. The cepstral technique in the presence of the diffuse component, converges to the true scatterer spacing only for regular scatterers with $\sigma=3.15\%$.

Figure 4 illustrates the range and effectiveness of the SAC function in estimating the mean-regular scatterer spacing from 0.5 to 1.35 mm, with a standard deviation of 9.99%, and -3 dB of the diffuse component to regular component strength. The SAC function converges to the true value of the mean-scatterer spacings for all the spacings in Fig. 4, with the estimates converging slower as the correlation peaks form closer to the PSD. The slower convergence for larger scatterer spacings results from greater errors in the phase correction factors. Since noise is included in these scans, the maximum value in a given window will sometimes be a peak from the diffuse scatterers, and as mentioned previously, this error more significantly affects the cases when only a few scatterers are in the processing window. The CV for the SAC function estimates remains within 5%–10% for all the cases shown, while the cepstral estimates have a CV>40%. These results along with the results in Fig. 3, show the dependence of the cepstral techniques on the high-pass filter cutoff frequency.

This section illustrates the estimation of the regular scatterer spacing in the presence of the diffuse component and variation in the regularity of the scatterer distribution. The SAC function estimates perform better than the cepstral estimates in the presence of the diffuse scattering component. The SAC function includes phase differences between the different spectral components, which in the presence of coherent scatterers produces well-defined spectral correlation peaks. The spectral correlation peaks are relatively insensitive to the diffuse components since these scatterers have a random phase distribution and their contributions average out. Cepstral techniques, on the other hand, do not utilize phase information and operate on the PSD characterization of the signal, which is directly affected by the diffuse scattering component.

III. EXPERIMENTAL RESULTS

In this section data from *in vivo* scans of liver tissue are used to illustrate the mean-scatterer spacing estimate using the SAC function and cepstral analysis. For real tissue the SAC function exhibits significant spectral correlation components due to the regularity in the tissue structure. B-scan images of the liver were obtained using the Ultramark 9 ultrasound system (ATL, Bothell, WA). Liver scans were obtained using a transducer with a center frequency $f_c=3.5$ MHz, 3-dB bandwidth $f_{3\ dB}=2.0$ MHz, and a sampling frequency $f_s=12$ MHz. The received signals were low-pass filtered (with a cutoff frequency of 6 MHz) before being sampled to prevent aliasing.
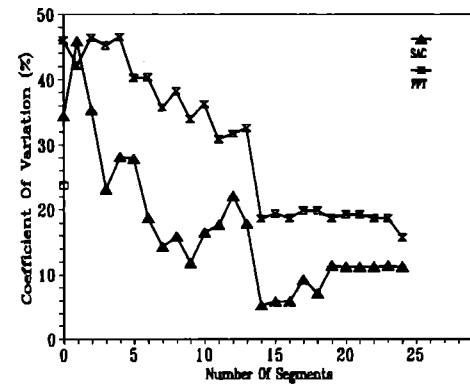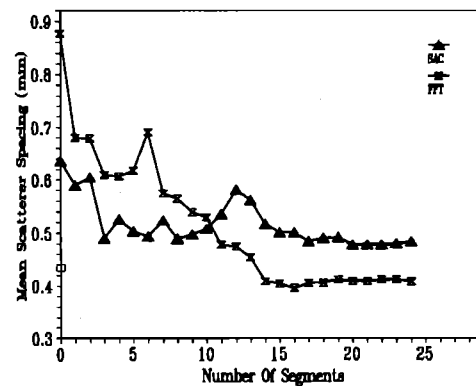
The basic functional unit of the liver is the liver lobule, which is a cylindrical structure several mm in length and
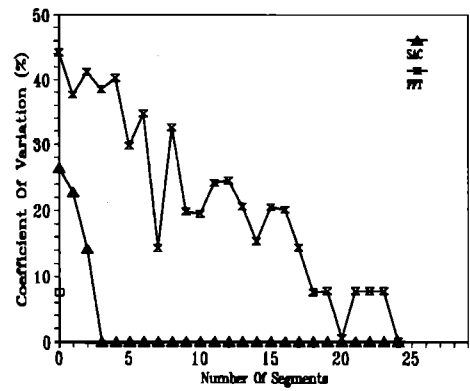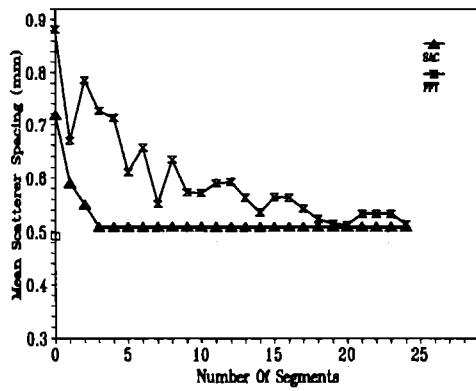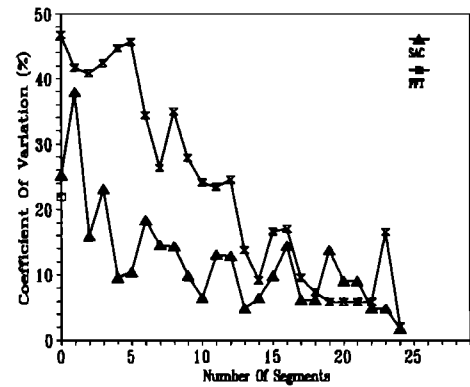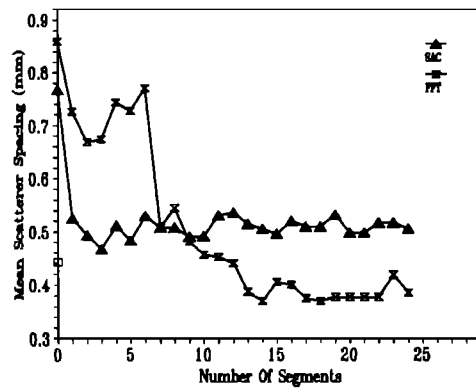
FIG. 3. Mean-scatterer spacing and the coefficient of variation for regular scatterers with spacing 0.51 mm, and +3 dB of diffuse scattering present. (a) Standard deviation 0.016 mm (3.15%), (b) standard deviation 0.051 mm (9.99%), (c) standard deviation 0.072 mm (14.14%).

0.8–2 mm in diameter. The human liver contains 50 000–100 000 individual lobules. The lobule is constructed around a central vein, and is composed of hepatic plates that radiate centrifugally from the central vein-like spokes in a wheel. The hepatic plates are separated by hepatic sinusoids which link the central vein to the portal venules. Each individual lobule is separated by a septa which contains the terminal bile ducts, portal venules, and the hepatic arterioles. Each hepatic plate is usually two cells thick, with bile canaliculi

between adjacent cells, which link to the terminal bile ducts.[20]

The SAC function and the cepstrum were obtained using the Welch–Bartlett technique with a 50% overlap of the windowed axial data segments of duration 10.67 μs (128 sample points or an 8-mm-data segment).[18] A set of segments were taken from a section of the liver sector scan that corresponded to a homogeneous appearance in the intensity image. The dimensions of the section were 16.47 mm in the
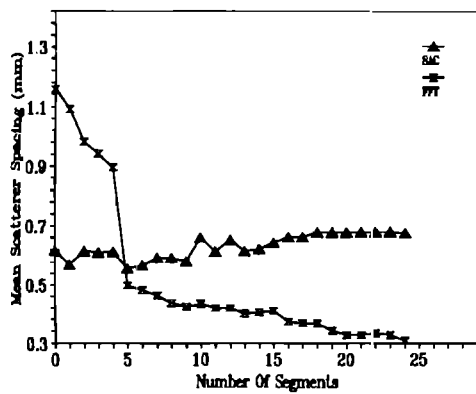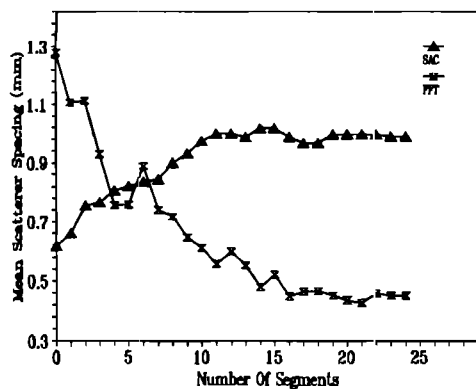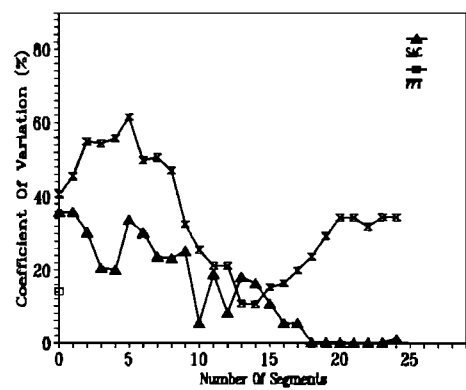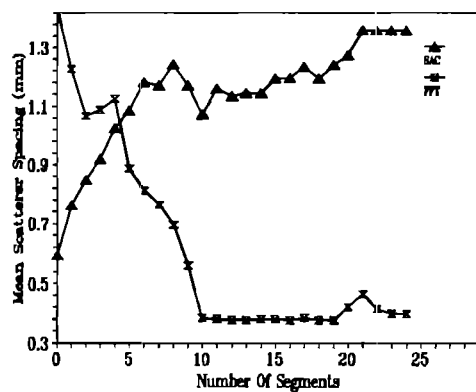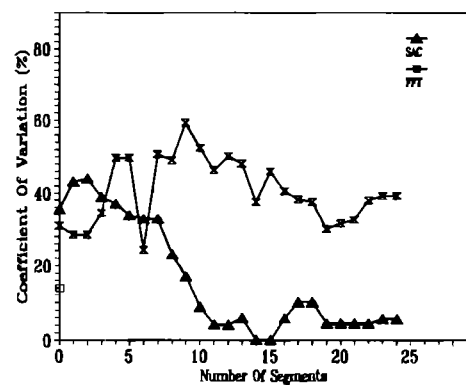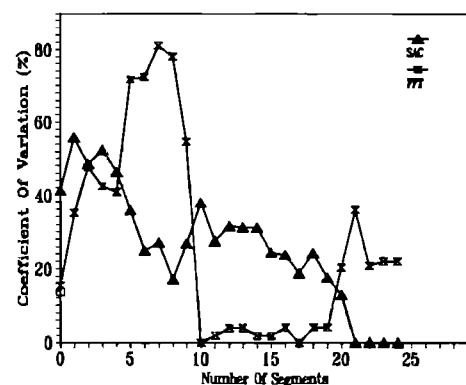
FIG. 4. Mean-scatterer spacing and the coefficient of variation for regular scatterers with standard deviation of 9.99% and −3 dB of the diffuse component. (a) Mean-scatterer spacing of 0.68 mm. (b) Mean-scatterer spacing of 1.02 mm. (c) Mean-scatterer spacing of 1.35 mm.

axial direction and 2.34° in the lateral direction (5 adjacent A-scans). This tissue section corresponds to an area of approximately 1.64 cm axially and 0.6 cm laterally. The SAC function and cepstral estimates are presented in Fig. 5.

The normalized SAC function and the cepstrum are obtained by averaging 15 individual SAC functions and periodigrams. The largest spectral correlation peak at (3.18,2.43) MHz in Fig. 5(a), corresponds to a scatterer spacing of 1.02 mm. Two other correlation peaks at (3.0,2.7) MHz and (3.56,2.9) MHz correspond to scatterer spacings of 2.56 and

1.16 mm, respectively. The 2.56-mm spacing is harmonically related to the 1.02-mm spacing (i.e., periodicity from scatterers clustered 2 at a time). Although a 2.04-mm spacing is expected in this case, there is increased error associated with this peak due to an increased (doubled) variance in the spacing and significance leakage from the PSD values. As a result, the peak is not as sharp or as high as the one corresponding to the fundamental scatterer spacing. The correlation peak due to the dominant spacing is about 15.6% stronger than the peak due to the spacing of 2.56 mm, and

T. Varghese and K. D. Donohue: Mean scatterer spacing estimates
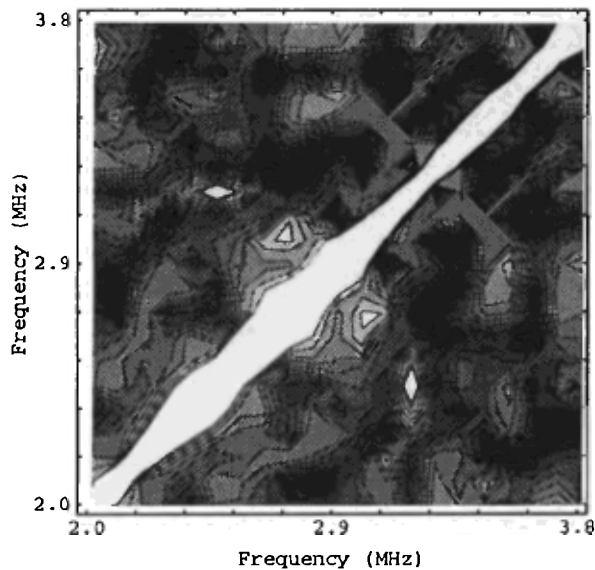
(a)
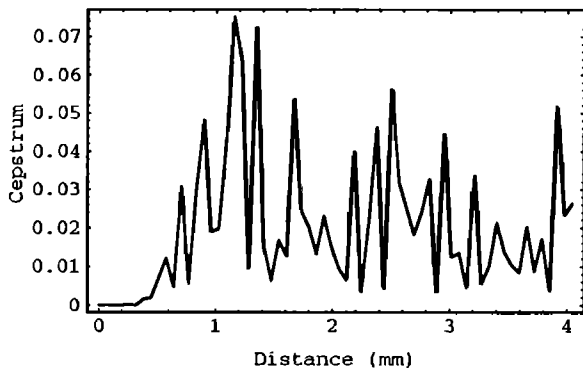
(b)

FIG. 5. (a) Spectral autocorrelation function and, (b) FFT cepstrum for liver tissue.

21.4% stronger than the peak due to the 1.16-mm spacing.

The FFT cepstrum in Fig. 5(b) shows the dominant peak due to a scatterer spacing of 1.21 mm, which is about 4.24% stronger than the next peak due to a 1.4-mm-scatterer spacing. Based on the convergence results of the previous section, the SAC function estimate is considered more reliable. While both estimates are close to one another, the cepstrum has more spurious peaks that compete with the dominate peak.

IV. CONCLUSION

This paper presented a quantitative method of estimating the mean-scatterer spacing using the SAC function. This technique is compared to the standard method of using the cepstrum to estimate the scatterer spacing. Significant performance improvements are obtained using the SAC function when compared to the cepstral technique in the presence of the diffuse scattering component. The cepstral technique also has the disadvantage of requiring *a priori* knowledge of the cutoff frequency to reduce the system effect from the tissue signature. The algorithm using the SAC function does not require a high-pass filter.

The mean-scatterer spacings detected by the SAC function is limited by the bandwidth of the pulse and the proximity of the spectral correlation peaks to the PSD. The technique using the SAC function cannot detect spectral peaks which are close (larger periodicities) to the main diagonal (PSD), since the spectral peak caused by the periodicity merges with the PSD due to the leakage from the finite window. This problem can be mitigated in the case of the SAC function, by using larger gate lengths to detect larger periodicities. The SAC function is a robust technique that is relatively insensitive to presence of diffuse (unresolvable) scatterers and the system effect. Cepstral methods rely on the assumption that the system effect is a slowly varying component and can be reduced by high-pass filtering. However, for *in vivo* analysis a total separation of the system effect from the tissue signature will not be obtained because of overlying tissue and the weighting from the scatterer position within the beam profile.

[1] M. F. Insana, R. F. Wagner, D. G. Brown, and T. J. Hall, "Describing small-scale structure in random media using pulse-echo ultrasound," J. Acoust. Soc. Am. **87**, 179–192 (1990).

[2] W. A. Gardner, "Exploitation of spectral redundancy in cyclostationary signals," IEEE Signal Proc. Mag. **8**, 14–36 (1991).

[3] K. D. Donohue and T. Varghese, "Spectral cross-correlation for tissue characterization," IEEE Ultrason. Symp. **2**, 1049–1052 (1992).

[4] T. Varghese and K. D. Donohue, "Characterization of tissue microstructure scatterer distribution with spectral correlation," Ultrasound Imag. **15**, 238–254 (1993).

[5] T. Varghese, "Detection of tissue microstructure anomalies with the spectral cross-correlation function: A simulation study," M.S. thesis, University of Kentucky, Lexington, KY, 1992).

[6] K. D. Donohue, J. M. Bressler, T. Varghese, and N. M. Bilgutay, "Spectral correlation in ultrasonic pulse-echo signal processing," IEEE Trans. Ultrason. Ferroel. Freq. Cont. UFFC-40, 330 337 (1993).

[7] K. D. Donohue, "Maximum-likelihood estimation of A-scan amplitudes for coherent targets in media of unresolvable scatterers," IEEE Trans. Ultrason. Ferroel. Freq. Cont. UFFC-39, 422–430 (1992).

[8] L. L. Fellingham and P. G. Sommer, "Ultrasonic characterization of tissue structure in the *in vivo* human liver and spleen," IEEE Trans. Sonics Ultrason. SU-31, 418–428 (1984).

[9] R. Kuc, K. Haghkerder, and M. O'Donnel, "Presence of cepstral peaks in random reflected ultrasound signal," Ultrason. Imag. **8**, 196–212 (1986).

[10] K. A. Wear, R. F. Wagner, M. F. Insana, and T. J. Hall, "Application of auto-regressive spectral analysis to cepstral estimation of mean scatterer spacing," IEEE Trans. Ultrason. Ferroel. Freq. Cont. **UFFC-40**, 50–59 (1993).

[11] R. F. Wagner, M. F. Insana, and D. G. Brown, "Unified approach to the detection and classification of speckle texture in diagnostic ultrasound," Opt. Eng. **25** 738–742 (1986).

[12] M. F. Insana, R. F. Wagner, B. S. Garra, D. G. Brown, and T. H. Shawker, "Analysis of ultrasound image texture via generalized Rician statistics," Opt. Eng. **25**, 743–748 (1986).

[13] L. Landini and L. Verrazzani, "Spectral characterization of tissue microstructure by ultrasound: A stochastic approach," IEEE Trans. Ultrason. Ferroel. Freq. Cont. **UFFC-37**, 448–456 (1990).

[14] J. G. Proakis, and D. G. Manolakis, Digital signal processing, Principles Algorithms and Applications, 2nd ed. (Macmillan, New York, 1992).

[15] L. R. Romijn, J. M. Thijssen, and G. W. J. Van Beuningen, "Estimation of scatterer size from back-scattered ultrasound: A simulation study," IEEE Trans. Ultrason. Ferroel. Freq. Cont. **UFFC-36**, 593–605 (1989).

[16] J. C. Bamber, "Theoretical modeling of the acoustic scattering structure of human liver," Acoust. Lett. **3**, 114–119 (1979).

[17] D. Nicholas, "Evaluation of back-scattering coefficients for excised human tissue: results, interpretation and associated measurements," Ultrasound Med. Bio. **8**, 17–28 (1982).

[18] P. D. Welch, "The use of fast Fourier transforms for the estimation of power spectra: A method based on time averaging over short modified periodigrams," IEEE Trans. Audio Electroacoust. **AU-15**, 70–73 (1967).

[19] A. Papoulis, *Probability Random, Variables, and Stochastic Processes*, 2nd ed. (McGraw-Hill, New York, 1984).

[20] A. C. Guyton, *Text book of Medical Physiology*, 4th ed. (W. B. Saunders, Philadelphia, 1971).

[21] W. A. Gardner, *Statistical Spectral Analysis* (Prentice-Hall, Englewood Cliffs, NJ, 1988).

[22] K. D. Donohue, T. Varghese, and N. M. Bilgutay, "Spectral redundancy in characterizing scatterer structures from ultrasonic echoes," *Review of Prog. Quant. Nondest. Eval.*, edited by D. O. Thompson and D. E. Chimenti (Plenum, New York, 1994), p. 13.